



# Modeling and understanding locomotion of pneumatic soft robots

Ning An, Meie Li & Jinxiong Zhou

To cite this article: Ning An, Meie Li & Jinxiong Zhou (2018): Modeling and understanding locomotion of pneumatic soft robots, *Soft Materials*, DOI: [10.1080/1539445X.2018.1460379](https://doi.org/10.1080/1539445X.2018.1460379)

To link to this article: <https://doi.org/10.1080/1539445X.2018.1460379>



Published online: 09 Apr 2018.



Submit your article to this journal [↗](#)



View related articles [↗](#)



View Crossmark data [↗](#)



## Modeling and understanding locomotion of pneumatic soft robots

Ning An<sup>a</sup>, Meie Li<sup>b</sup>, and Jinxiong Zhou<sup>a</sup>

<sup>a</sup>State Key Laboratory for Strength and Vibration of Mechanical Structures and School of Aerospace, Xi'an Jiaotong University, Xi'an, China;

<sup>b</sup>State Key Laboratory for Mechanical Behavior of Materials, School of Materials Science and Engineering, Xi'an Jiaotong University, Xi'an, China

### ABSTRACT

Imitating natural locomotion of biological systems (soft-bodied animals) opens the door to the development of a new class of machine, referring to soft robots. A variety of soft robots have been demonstrated by researchers and engineers through incorporating soft technologies into their designs. Yet computer modeling of locomotion of soft robots remains to be a challenging task, not merely because their intrinsic deformation is continuous, complex, and highly nonlinear compared to conventional rigid-bodied robots, but moreover because of the complicated contact problems encountered during locomotion of soft robotics. Herein, we present a combined analytical and numerical analysis of the locomotion of pneumatic network-based soft robots. Concerning a quadruped robot, two fundamental different gaits (undulation and crawling) were identified and numerically validated by two driving modes of pneumatic robots. Extracting ground reaction forces and centroid trajectory from the simulation throws a light on the underlying mechanism of locomotion of soft robots. Our efforts would enhance the understanding and facilitate the control, manipulation, and trajectory optimization of bio-inspired soft robots.

### ARTICLE HISTORY

Received 17 August 2017  
Accepted 4 March 2018

### KEYWORDS

Crawling; finite element method; pneumatic networks; soft robot; undulation


## Introduction

Natural locomotion of soft-bodied animals has long been a source of inspiration for making soft robots (1–3). Various bio-inspired soft mobile robots were demonstrated by robotics researchers and engineers through mimicking the locomotion of soft-bodied animals; typical examples include caterpillar-inspired robots (4), multigait quadruped (5,6), worm-inspired robots (7–9), snake-inspired systems (10), manta ray-inspired robots (11), and jellyfish-like robots (12,13), etc. In particular, pneumatically powered soft robots are promising candidates for robotics applications because of their ease and low cost of design and fabrication; furthermore, pneumatic soft robots can be lightweight, environmentally benign, and easily actuated (6,14).

However, unlike the control of rigid robots, whose movements can be described using six degrees of freedom (three rotations and three translations about the  $x$ ,  $y$ , and  $z$  axes), the locomotion of soft robots is continuous and thus exhibits infinite degrees of freedom. In theory, the final shape of the robot can be determined by a continuous function, and modeling this behavior requires continuous mechanics. One proposed approach is to simplify a soft robot into an elastic rod and a rigid mass, and using

a modified Euler's theory to predict locomotion by controlling the intrinsic curvature (15); another strikes a balance between the extremes of rigid-body and continuous mechanics simulation and develops a planar, extensible-link approach, that is, using a series of deformable links connected by revolute joints to capture the crawling locomotion of caterpillar-inspired soft robots (16); and other researchers present approaches to treat the kinematics of trunk-like continuum robot as an inverse dynamics problem (17,18). A limitation of existing analytical approaches to capture the locomotion of robots is that the local mechanical deformation is not considered in the solution, and thus these models do not capture all aspects of soft bodies during locomotion.

Local mechanical deformation is crucial for pneumatic network (PN)-based soft robotics. It is the unsymmetry of material distribution and the unsymmetric mechanical deformation upon pressurization of PN that causes the bending (14,19,20), twisting (21), and eventually locomotion (5,6,22) of pneumatically powered soft robots. To address this issue, researchers employed finite element method (FEM) to understand and predict behavior of PN, bending and twisting (19,21,23), for example, and the FE simulations were

**CONTACT** Jinxiong Zhou ✉ [jxzhouxx@mail.xjtu.edu.cn](mailto:jxzhouxx@mail.xjtu.edu.cn)  State Key Laboratory for Strength and Vibration of Mechanical Structures and School of Aerospace, Xi'an Jiaotong University, Xi'an 710049, China.

Color versions of one or more of the figures in the article can be found online at [www.tandfonline.com/lsfm](http://www.tandfonline.com/lsfm).

validated by experimental data. Another important issue for modeling the locomotion of pneumatic soft robots is the contact problem. For example, Majidi et al. pointed out that interfacial tractions play a unique role in controlling both the speed and the direction of soft robots (24). Perhaps because of this perceived difficulty of solving the inevitable contact problem between soft body and ground (25,26), no prior attempts have been made to model the locomotion of pneumatic soft robots using FE models.

In this contribution, we report our efforts to understand the locomotion of pneumatic soft robotics through a combination of analytical analysis and FEM simulation. Our simulations were all implemented in a widely available commercial finite element software, ABAQUS 6.14 (Simulia, Providence, RI), which would facilitate interaction between industry and academia. The bending deformation of a single-segment bilayer PN beam was studied via a model analysis. A 2D simplified robotic model as well as a 3D realistic PN-based soft robot was constructed with multiple PN channels embedded and multiple contacts accounted for. Two fundamental locomotions (undulation and crawling) are elucidated by two different driving modes with the help of contact forces and variation of center of mass extracted from FEM simulation. Our simulations and analysis shed light on the locomotion mechanics of such soft robots and would aid the design and optimization of complex pneumatic soft robots.

## Model analysis

We present a theoretical model to describe the inflation pressure versus bending curvature of a single PN segment. As schematized in Fig. 1, the PN segment consists

of two layers, a set of soft Ecoflex channels (green) and a thin layer of strain-limiting PDMS elastomer (blue), and both are treated as incompressible hyperelastic materials (6,14). For the sake of analytical simplicity, we have assumed all the pneumatic channels to be circular and to have infinite length along the direction perpendicular to the page. Plane strain conditions are adopted and finite deformation is considered.

Each single pneumatic channel in Fig. 1 will expand its volume upon pressurization, thus the length of the actuating layer of PN elongates due to actuation. To accommodate the mismatch between the actuating and the strain-limiting layers, the bilayer PN segment bends to the strain-limiting layer. The thickness of the strain-limiting layer ( $<0.2$  mm) is much less than the thickness of pneumatic channels, and thus its bending modulus can be ignored; meanwhile, the initial shear modulus of PDMS is much larger than that of Ecoflex, then the length of strain-limiting layer can be considered to be unchanged during the bending process.

From Fig. 1 the following geometrical relations are derived when the PN beam bends from original (Fig. 1 (a)) to current state (Fig. 1(b)),

$$L = n \cdot 2R_2 = R_S \cdot \theta \quad (1)$$

$$l = n \cdot 2r_2 = (R_S + r_2) \cdot \theta \quad (2)$$

where  $L$  is the initial length in lateral direction of both actuating layer and strain-limiting layer,  $l$  is the length in lateral direction of actuating layer upon pressurization,  $n$  is the number of pneumatic channels,  $R_2$  is the outer radius of pneumatic channels in the reference state,  $r_2$  is the outer radius of pneumatic channels in the equilibrium state,  $R_S$  is the radius of curvature of

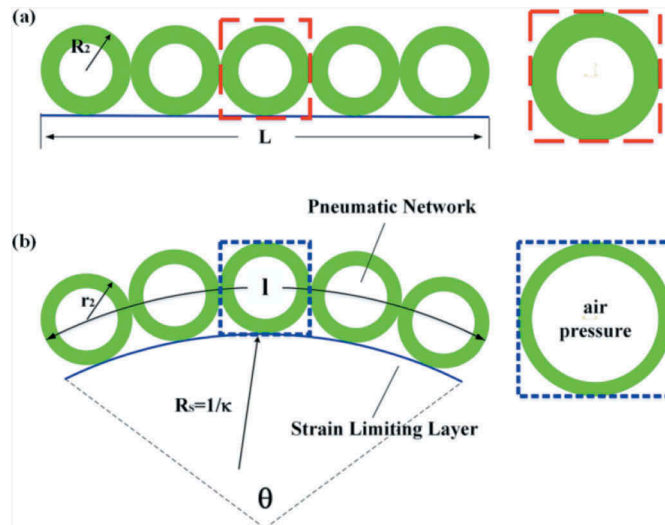


**Figure 1.** Geometry of a single bilayer PN segment in (a) the reference state and (b) the current state.

the strain-limiting layer in the equilibrium state, and  $\theta$  represents the bending angle.

The combination of Eqs. (1) and (2) gives an analytical expression for the curvature of the strain-limiting layer, i.e.,

$$\kappa = \frac{1}{R_s} = \frac{1}{R_2} - \frac{1}{r_2} \quad (3)$$

where  $r_2$  can be determined by solving the boundary value problem of homogeneous inflation of a planar hyperelastic thick-walled annulus (27). Considering an annulus made of incompressible neo-Hookean material with initial shear modulus  $\mu$  is subject to uniform inflation pressure  $p$ , and invoking the mechanical equilibrium conditions gives the following explicit forms for radial stress and displacement:

$$\sigma_r = -\mu(\ln r + C_1 r^{-2} - \frac{1}{2} \ln(r^2 - 2C_1)) + C_2 \quad (4)$$

$$r^2 = R^2 + 2C_1 \quad (5)$$

where  $R$  and  $r$  represent the radial coordinates of a material particle in the reference and inflated configuration, respectively. Two constants,  $C_1$  and  $C_2$  in Eqs. (4) and (5), can be determined by considering the boundary conditions that  $\sigma_r$  is equal to inflation pressure  $p$  on the inner surface, and vanishes on the outer free surface. Figure 2 plots the comparison between the theoretical and FEM solutions for the bending curvature versus inflation pressure relation. As shown in the snapshots of deformation inserted in Fig. 2, a pneumatic bilayer beam consists of an actuating Ecoflex layer with embedded pneumatic

channels and a strain-limiting PDMS layer. When pressurized, the actuator undergoes a bending deformation.

### Finite element modeling

The theoretical model gains insights into the bending response of a single bilayer PN segment upon pressurization. It is, however, hard to unveil the local deformation of the soft robotics and in particular the contact forces between the soft body and the ground, which is crucial for understanding the locomotion of soft robots. In case of fixed contact conditions, the normal contact force between the soft body and the ground resulting from gravity determines the maximum possible friction force, which governs the tendency of sliding and thus the means of locomotion (24). FEM modeling, on the other hand, is capable of capturing more detailed local deformation of pneumatic soft robots as well as the variation of contact forces during locomotion (14,28–31). In addition, a better understanding of the locomotion process is elucidated via the powerful postprocessing and computer visualization of commercial FEM software.

### Two-dimensional bilayer PN beam

We extend the single segment into a bilayer triple-segment PN (denoted as PN1, PN2, and PN3) beam model shown in Fig. 3, which can be pressurized and actuated independently. The triple-segment beam was discretized by 19688 linear quadrilateral plain strain

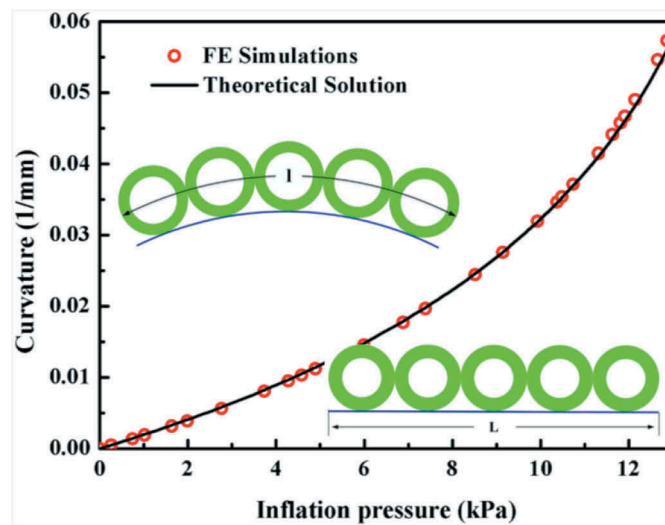


**Figure 2.** Comparison of FE simulations and theoretical solution of bending curvature of a pneumatic bending beam. A pneumatic bilayer beam consists of an actuating Ecoflex layer embedded pneumatic channels and a strain-limiting PDMS layer. When pressurized, the actuator undergoes a bending deformation. The inner and outer radius of pneumatic channels in the reference state are 3 and 5 mm, respectively; the initial shear modulus  $\mu$  of Ecoflex and PDMS were set to be 0.03 and 1.84 MPa, respectively.

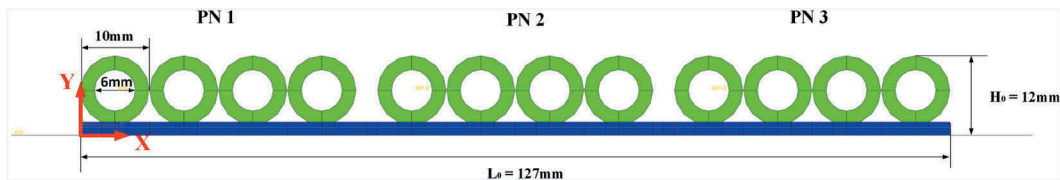


**Figure 3.** Two-dimensional bilayer PN beam, along with length scales and materials distribution. The pneumatic networks are divided into three parts (PN1, PN2, and PN3), which can be pressurized independently. The green part represents Ecoflex layers, and the blue one represents PDMS layer.

elements (CPE4H in ABAQUS). What makes the model in Fig. 3 different from that in Fig. 1 is the contact between the PN beam and the ground is accounted for. The ground was treated as rigid body and discretized by 1000 linear line elements of type R2D2. Two typical shear moduli,  $\mu = 0.03$  MPa for Ecoflex and  $\mu = 1.84$  MPa for PDMS (21), were set in simulation. The fluid cavity capability provided in ABAQUS was adopted to model the pressure exerted on the inner surface of the annulus (32). Frictional surface to surface contact type was employed between the main body and ground, and the “node to surface” discretization method was chosen for improving convergence. The penalty contact algorithm was adopted, and the coefficient of friction is set as 0.7.

Figure 4 shows one complete cycle of pressurization and depressurization of the triple-segment PN

beam with contact that results in undulation locomotion, and Fig. 5(a) plots the variation of contact forces – the resultant contact forces due to normal contact pressure – between main soft body and the ground during cycle. To be specific, the undulation locomotion was realized through the following sequence of steps: (i) applying gravity to the main body for maintaining stable contact between main body and ground and generating uniform normal contact forces, approximately 5 mN. (ii) Pressurizing PN1 up to a pressure 13 kPa lifts the rear leg, reduces the contact force between rear leg and ground to 2.5 mN, and increases that between front leg and ground to 7.5 mN due to shifting of center of gravity. (iii) Pressurizing PN2 (13 kPa) lifts the main body further and pulls forward the rear leg; the front leg remains stationary because contact force between front leg and ground is larger than that

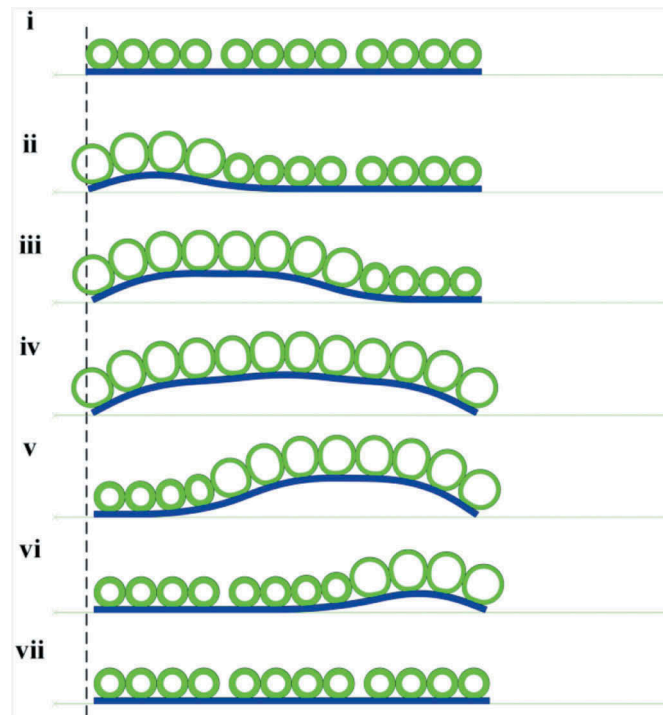


**Figure 4.** Modeling one complete cycle of pressurization and depressurization of PNs with contacts that results in undulation (2D FEM model).



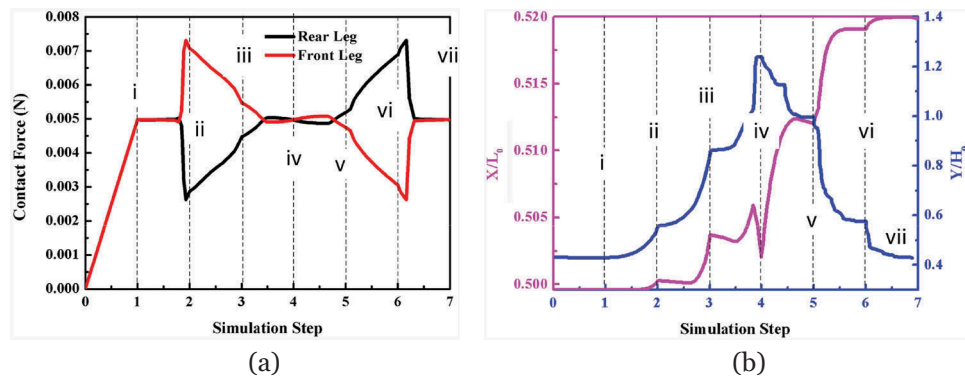


**Figure 5.** (a) Variation of contact forces between main soft body and the ground during the whole actuating cycle. (b) Position of the center of mass of the soft robot during actuating cycle (2D FEM model). The magenta and blue curves represent the variation of coordinates of the center of mass,  $X$  and  $Y$ , normalized by the initial length  $L_0$  and the initial height  $H_0$ , respectively. The  $X$ -coordinate of the center of mass shows an overall increasing tendency from step i to vii, implying a forward motion in the direction of positive  $X$ -axis; the going down in step iv is caused by sliding of the front leg tip to the left when it is pressurized in step iv. The  $Y$ -coordinate of the center of mass shows a trend of going up firstly and then going down, corresponding to the undulatory locomotion mode shown in Figure 4.

between the rear leg and ground. (iv) Pressurizing PN3 by the same pressure 13 kPa lifts the front leg and entails a new stable configuration of the beam with equal rear and front contact forces. (v) Depressurizing of PN1 puts down the rear leg and pushes the robot ahead; contact force between rear leg and ground exceeds that between front leg and ground gradually. (vi) Depressurization of PN2 puts down the body; the rear leg remains stationary while the front one is pushed ahead because the former maintains larger contact force in contact with ground. (vii) Depressurization of PN3 puts down the front leg; the main body arrives at initial stable state but has been pulled forward after a complete cycle of pressurization and depressurization. As shown in Fig. 4, each leg may either be in point contact with the ground or be flattened and in “surface contact” over a finite area. For example, in the actuating configuration shown in Fig. 4(iii), the rear leg is in point contact with the ground whereas the front leg is in surface contact with the ground, and vice versa in Fig. 4(v). The variation of magnitude of contact forces in Fig. 5(a) is caused by shifting of center of gravity during the cycle, which is monitored and plotted in Fig. 5(b).

### Three-dimensional soft robot model

Laying our basis on the previously mentioned model analysis and 2D FEM simulation, we move further to model a realistic 3D pneumatic multigait soft robot developed by (6). The 3D geometry of the soft robot along with length scales is shown in Fig. 6(a). The robot is composed of five independent PNs: two rear

legs are composed of PN1 and PN2, the central body consists of PN5, and PN3 and PN4 constitute the two front legs. The dimensions of the pneumatic soft robot are  $135.7\text{mm} \times 58.5\text{mm} \times 6.3\text{mm}$ ; the thicknesses of Ecoflex layer and PDMS layer is 5.3 and 1 mm, respectively, the depth of each channel is 4 mm, the thickness of each channel is 1.5 mm, and the distance between two adjacent channels is 2 mm. More than 170,000 linear hybrid elements (C3D8H and C3D6H) were generated to model the soft robot, and once again the ground was modeled as rigid body. The detailed meshing is demonstrated in Fig. 6(b), and accuracy of simulation is ascertained through meshing refinement scheme. Figure 6(c) shows the bending deformation of the rear legs upon an inflated pressure of 0.02 MPa. Similar to the undulation modeling of 2D PN beam, Figs. 7 and 8 present the undulatory locomotion of 3D robot upon one cycle of pressurization and depressurization.

Finally, we explore another different locomotion mode, crawling locomotion, which is realized by a different driving mode. As illustrated in Figs. 9 and 10, the crawling locomotion consists of the following sequence actuation steps: (i) applying gravity to the soft robot and generating uniform normal contact forces between the robot and ground, approximately 0.12 N as extracted from FEM simulation. (ii) Pressuring PN5 by a pressure 0.02 MPa lifts the core of the robot away the ground. The  $Y$ -coordinate of the center of mass of the robot goes up due to the lifting of the core of the robot. The two rear legs and the two front legs process the same contact force, 0.12 N, as extracted from

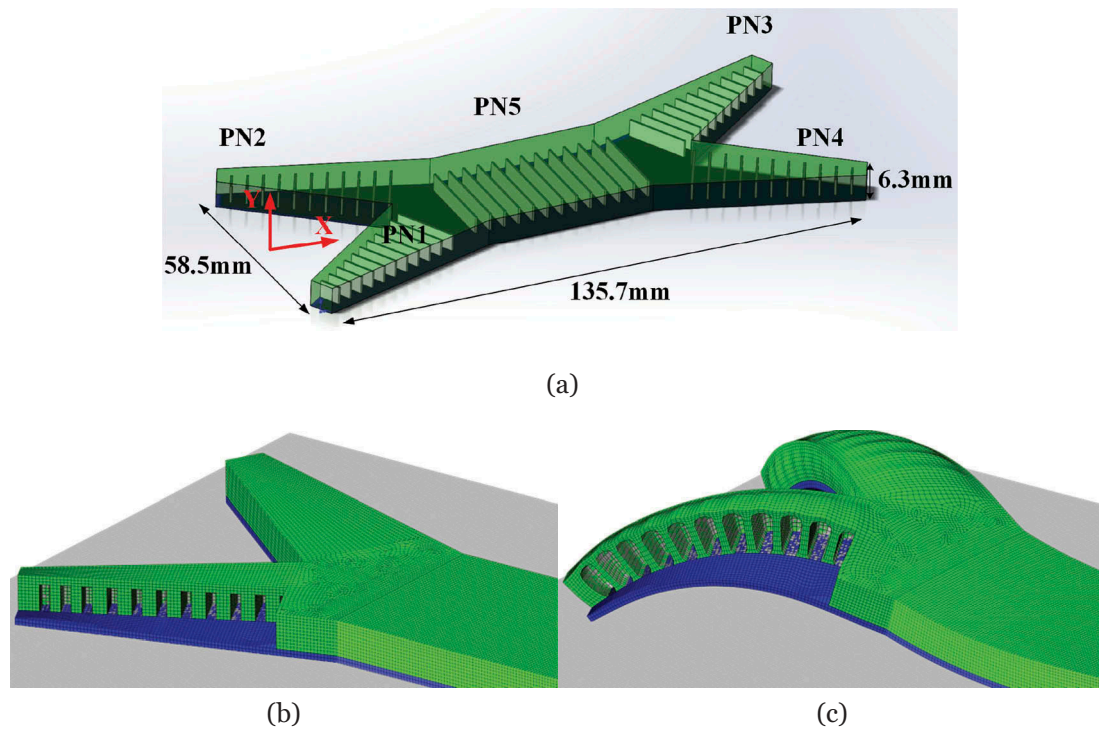


**Figure 6.** (a) Schematic representation of a PN-based soft robot. The independent PNs are labeled as PN1, 2, 3, 4, and 5. (b) FE mesh and material distribution. The model was discretized by 172844 linear hexahedral elements (C3D8H) and 546 linear wedge elements (C3D6H). The green solids are Ecoflex layers, the blue layer is PDMS, and the gray space represents the underlying ground. (c) Snapshot of the deformation of the rear leg of the robot upon applied inflation pressure of 0.02 MPa.

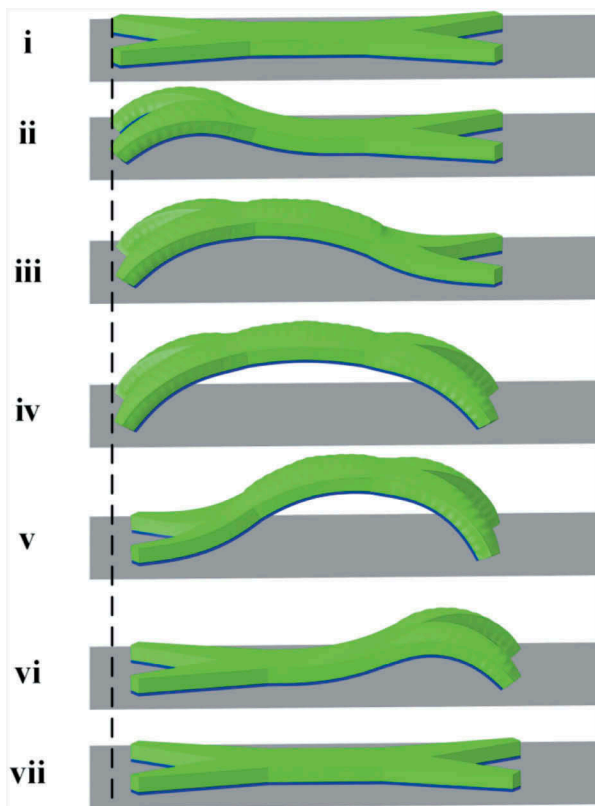


**Figure 7.** Cycle of pressurization and depressurization of PNs that result in undulation (3D FEM model).

simulation. (iii) Pressuring PN1 pulls the PN1 leg forward. (iv) Simultaneously pressurizing PN3 and depressurizing PN1 propels the body of robot forward, indicated by an increase of in the  $X$ -coordinate of the center of mass of the robot. (v) Pressurizing PN2 while depressurizing PN3 pulls the PN2 leg forward. (vi) Simultaneously pressurizing PN4 and depressurizing of PN2 propels the body of robot forward again, corresponding to a second marked increase in the  $X$ -coordinate of position of the center of mass of the robot. (vii) Pressurizing PN1 while depressurizing PN4 pulls the PN1 leg forward, and the main body arrives at another (iii) stage but has been pulled forward, thus creating an actuating cycle. Figure 10(a) and (b) gives the variation of contact forces and the center of mass during the locomotion of crawling.

### Concluding remarks

The field of soft robotics has attracted intensive attention and interest in both engineering and academia communities. A variety of manufacturing technologies and large number of prototypes of soft robotics have been developed and demonstrated in the past decade. In sharp contrast to the rapid

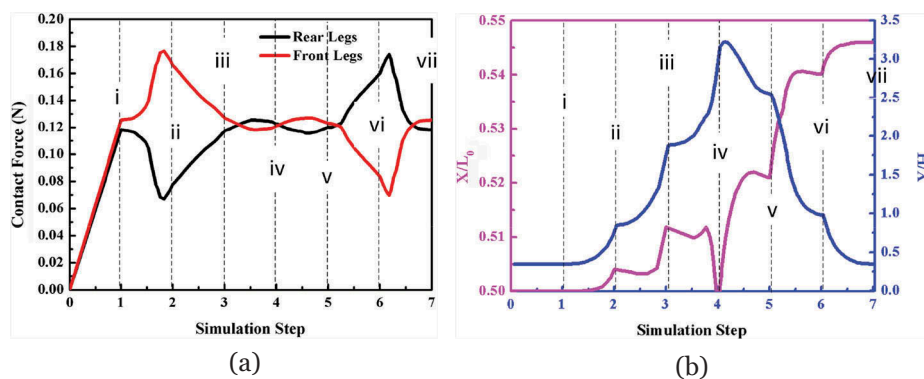


**Figure 8.** (a) Variation of contact forces between main soft body and the ground during the whole actuating cycle of undulation. Two rear legs are composed of PN1 and PN2, while PN3 and PN4 constitute two front legs. (b) Position of the center of mass of the soft robot during actuating cycle of undulation (3D FEM model). The magenta and blue curves represent the variation of coordinates of the center of mass,  $X$  and  $Y$ , normalized by the initial length  $L_0$  and the initial height  $H_0$ , respectively.

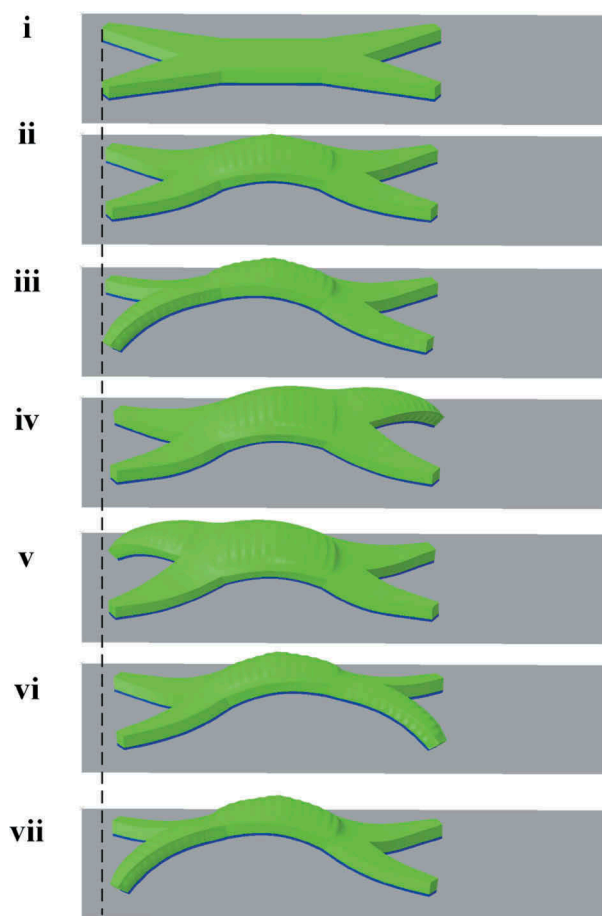


**Figure 9.** Cycle of pressurization and depressurization of PNs that result in crawling.

development of design and fabrication techniques of soft robotics, modeling and control of soft robotics remain as challenging tasks and the research is really scarce. The reasons and the technical difficulties are obvious: the soft robotics are made of soft materials, thus the motion and deformation of the soft robotics

is continuous and distributed all over the soft body in response to an applied external actuation. The manipulation of the locomotion of the soft robotics is much complicated as compared with their hard counterparts.

To aid the design and the control of soft robots, the understanding of their locomotion is essential. By choosing the recently intensively studied pneumatically driven soft robotics as a typical example, we investigate the locomotion of pneumatic soft robots through a combination of analytical analysis and numerical simulation. We present for the very first time the detailed local deformation, the variation of contact forces, and the changing of center of mass during the locomotion process. The local deformation of channels caused by pneumatic pressure is the fundamental source of the sequent bending behavior of PNs and is closely correlated to locomotion behavior of soft robots. Variation of contact forces and the associated variation of maximum friction forces govern the slipping tendency and thus the means of locomotion. Variation of contact forces is elucidated through our detailed local deformation analysis and is found to be attributed to variation of center of mass during the actuating cycle. The simulation results identify two fundamental locomotion processes of such robots, i.e., undulatory locomotion and crawling locomotion, which can be realized by different actuation modes. The numerical strategy and analysis procedure is generic and can be extended to study locomotion of other types of soft robotics albeit only pneumatic robots are considered in this paper. The use of commercial software would also facilitate interaction between industry and academia, and accelerate the development of soft robotics.



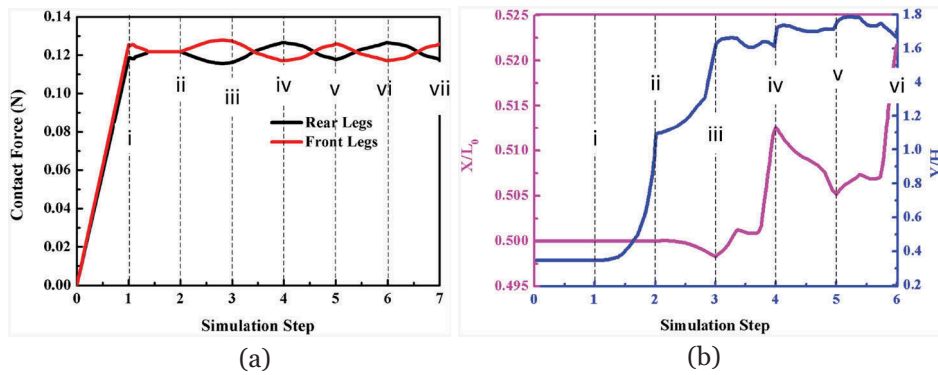


**Figure 10.** (a) Variation of contact forces between main soft body and the ground during the whole actuating cycle of crawling. (b) Position of the center of mass of the soft robot during actuating cycle of crawling. The magenta and blue curves represent the variation of coordinates of the center of mass,  $X$  and  $Y$ , normalized by the initial length  $L_0$  and the initial height  $H_0$ , respectively. The  $Y$ -coordinate of the center of mass goes up steeply from step i to iii, and then experiences some fluctuations, corresponding to the crawling locomotion mode shown in Figure 9.

## Funding

This work was supported by the Natural Science Foundation of China [Grants 11372239 and 11472210].

## References

- Trivedi, D., Rahn, C.D., Kier, W.M., and Walker, I.D. (2008) Soft robotics: biological inspiration, state of the art, and future research. *Applied Bionics and Biomechanics*, 5(3):99–117.
- Rus, D., and Tolley, M.T. (2015) Design, fabrication and control of soft robots. *Nature*, 521(7553):467–475.
- Kim, S., Laschi, C., and Trimmer, B. (2013) Soft robotics: a bioinspired evolution in robotics. *Trends in Biotechnology*, 31(5):287–294.
- Lin, H.T., Leisk, G.G., and Trimmer, B. (2011) GoQBot: a caterpillar-inspired soft-bodied rolling robot. *Bioinspiration & Biomimetics*, 6(2):026007.
- Morin, S.A., Shepherd, R.F., Kwok, S.W., Stokes, A.A., Nemiroski, A., and Whitesides, G.M. (2012) Camouflage and display for soft machines. *Science*, 337(6096):828–832.
- Shepherd, R.F., Ilievski, F., Choi, W., Morin, S.A., Stokes, A.A., Mazzeo, A.D., ... Whitesides, G.M. (2011) Multigait soft robot. *Proceedings of the National Academy of Sciences*, 108(51):20400–20403.
- Umedachi, T., Vikas, V., and Trimmer, B.A. (2016) Softworms: the design and control of non-pneumatic, 3D-printed, deformable robots. *Bioinspiration & Biomimetics*, 11(2):025001.
- Seok, S., Onal, C.D., Cho, K.J., Wood, R.J., Rus, D., and Kim, S. (2013) Meshworm: a peristaltic soft robot with antagonistic nickel titanium coil actuators. *IEEE/ASME Transactions on Mechatronics*, 18(5):1485–1497.
- Wang, W., Lee, J.Y., Rodrigue, H., Song, S.H., Chu, W. S., and Ahn, S.H. (2014) Locomotion of inchworm-inspired robot made of smart soft composite (SSC). *Bioinspiration & Biomimetics*, 9(4):046006.
- Onal, C.D., and Rus, D. (2013) Autonomous undulatory serpentine locomotion utilizing body dynamics of a fluidic soft robot. *Bioinspiration & Biomimetics*, 8(2):026003.
- Suzumori, K., Endo, S., Kanda, T., Kato, N., and Suzuki, H., 2007, April. A bending pneumatic rubber actuator realizing soft-bodied manta swimming robot. In *Proceedings 2007 IEEE International Conference on Robotics and Automation* (pp. 4975–4980). IEEE. Available from <http://ieeexplore.ieee.org/document/4209864/>
- Nawroth, J.C., Lee, H., Feinberg, A.W., Ripplinger, C. M., McCain, M.L., Grosberg, A., ... Parker, K.K. (2012) A tissue-engineered jellyfish with biomimetic propulsion. *Nature Biotechnology*, 30(8):792–797.
- Godaba, H., Li, J., Wang, Y., and Zhu, J. (2016) A soft jellyfish robot driven by a dielectric elastomer actuator. *IEEE Robotics and Automation Letters*, 1(2):624–631.
- Ilievski, F., Mazzeo, A.D., Shepherd, R.F., Chen, X., and Whitesides, G.M. (2011) Soft robotics for chemists. *Angewandte Chemie*, 123(8):1930–1935.
- Zhou, X., and Majidi, C. (2015) Flexing into motion: a locomotion mechanism for soft robots. *International Journal of Non-Linear Mechanics*, 74:7–17.
- Saunders, F., Trimmer, B.A., and Rife, J. (2010) modelling locomotion of a soft-bodied arthropod using inverse dynamics. *Bioinspiration & Biomimetics*, 6(1):016001.
- Neppalli, S., Csencsits, M.A., Jones, B.A., and Walker, I.D. (2009) Closed-form inverse kinematics for continuum manipulators. *Advanced Robotics*, 23(15):2077–2091.
- Jones, B.A., and Walker, I.D. (2006) Kinematics for multisection continuum robots. *IEEE Transactions on Robotics*, 22(1):43–55.
- Mosadegh, B., Polygerinos, P., Keplinger, C., Wennstedt, S., Shepherd, R.F., Gupta, U., ... Whitesides, G.M. (2014) Pneumatic networks for soft robotics that actuate rapidly. *Advanced Functional Materials*, 24(15):2163–2170.
- Martinez, R.V., Fish, C.R., Chen, X., and Whitesides, G.M. (2012) Elastomeric origami: programmable paper-elastomer composites as pneumatic actuators. *Advanced Functional Materials*, 22(7):1376–1384.

21. Martinez, R.V., Branch, J.L., Fish, C.R., Jin, L., Shepherd, R.F., Nunes, R., ... Whitesides, G.M. (2013) Robotic tentacles with three-dimensional mobility based on flexible elastomers. *Advanced Materials*, 25(2):205–212.
22. Tolley, M.T., Shepherd, R.F., Mosadegh, B., Galloway, K.C., Wehner, M., Karpelson, M., ... Whitesides, G.M. (2014) A resilient, untethered soft robot. *Soft Robotics*, 1(3):213–223.
23. Elsayed, Y., Lekakou, C., Geng, T., and Saaj, C.M., 2014, July. Design optimisation of soft silicone pneumatic actuators using finite element analysis. In *2014 IEEE/ASME International Conference on Advanced Intelligent Mechatronics* (pp. 44–49). IEEE. Available from <http://ieeexplore.ieee.org/document/6878044/>
24. Majidi, C., Shepherd, R.F., Kramer, R.K., Whitesides, G.M., and Wood, R.J. (2013) Influence of surface traction on soft robot undulation. *The International Journal of Robotics Research*, 32(13):1577–1584.
25. Yang, Z., Zhu, L., Li, B., Sun, S., Chen, Y., Yan, Y., ... Chen, X., 2016. Mechanical design and analysis of a crawling locomotion enabled by a laminated beam. *Extreme Mechanics Letters*.
26. Xydas, N., Bhagavat, M., and Kao, I. (2000) Study of soft-finger contact mechanics using finite elements analysis and experiments. In *Robotics and Automation, 2000. Proceedings. ICRA'00. IEEE International Conference On.* (Vol. 3, pp. 2179–2184). IEEE. Available from <http://ieeexplore.ieee.org/document/846351/>
27. Ogden, R.W. (1997) *Non-Linear Elastic Deformations*; Courier Corporation. INC, New York: Dover Publications.
28. An, N., Li, M., and Zhou, J. (2015) Instability of liquid crystal elastomers. *Smart Materials and Structures*, 25(1):015016.
29. He, T., Li, M., and Zhou, J. (2012) modelling deformation and contacts of pH sensitive hydrogels for microfluidic flow control. *Soft Matter*, 8(11):3083–3089.
30. Boyce, M.C., and Arruda, E.M. (2000) Constitutive models of rubber elasticity: a review. *Rubber Chemistry and Technology*, 73(3):504–523.
31. Nicholson, D.W., and Nelson, N.W. (1990) Finite-element analysis in design with rubber. *Rubber Chemistry and Technology*, 63(3):368–406.
32. Duncanson, W.J., Kodger, T.E., Babaei, S., Gonzalez, G., Weitz, D.A., and Bertoldi, K. (2015) Microfluidic fabrication and micromechanics of permeable and impermeable elastomeric microbubbles. *Langmuir*, 31(11):3489–3493.